Advances in Applied Mathematics and Mechanics
Adv. Appl. Math. Mech., Vol. **9**, No. 4, pp. 1012-1034

DOI: 10.4208/aamm.2016.m1477
August 2017

Effect of Nonuniform Grids on High-Order Finite Difference Method

Dan Xu[1,*], Xiaogang Deng[1], Yaming Chen[2], Guangxue Wang[3] and Yidao Dong[1]

[1] *College of Aerospace Science and Engineering, National University of Defense Technology, Changsha, Hunan 410073, China*
[2] *College of Science, National University of Defense Technology, Changsha, Hunan 410073, China*
[3] *School of Physics, Sun Yat-sen University, Guangzhou, Guangdong 510006, China*

Received 1 March 2016; Accepted (in revised version) 20 September 2016

Abstract. The finite difference (FD) method is popular in the computational fluid dynamics and widely used in various flow simulations. Most of the FD schemes are developed on the uniform Cartesian grids; however, the use of nonuniform or curvilinear grids is inevitable for adapting to the complex configurations and the coordinate transformation is usually adopted. Therefore the question that whether the characteristics of the numerical schemes evaluated on the uniform grids can be preserved on the nonuniform grids arises, which is seldom discussed. Based on the one-dimensional wave equation, this paper systematically studies the characteristics of the high-order FD schemes on nonuniform grids, including the order of accuracy, resolution characteristics and the numerical stability. Especially, the Fourier analysis involving the metrics is presented for the first time and the relation between the resolution of numerical schemes and the stretching ratio of grids is discussed. Analysis shows that for smooth varying grids, these characteristics can be generally preserved after the coordinate transformation. Numerical tests also validate our conclusions.

AMS subject classifications: 65N06, 65N22

Key words: Finite difference method, nonuniform grids, coordinate transformation, Fourier analysis.

1 Introduction

The FD method is historically old and plays an important role in the computational fluid dynamics [1]. In recent 20 years, due to the efficiency and simplicity, various high-order

*Corresponding author.
Email: xudan5293417@yahoo.com (D. Xu)

 ©2017 Global Science Press

https://doi.org/10.4208/aamm.2016.m1477 Published online by Cambridge University Press

schemes based on the FD method have been proposed and widely used in direct numerical simulations (DNS), computational aeroacoustics (CAA) and large eddy simulations (LES), in which the high resolution is needed. At present, the high-order FD method has been successfully applied in the simulations of incompressible, compressible and hypersonic flows [2–4] and several other practical applications [5,6].

In the studies of high-order FD method, different discretization techniques for the spatial derivative are developed. The common one is the explicit scheme which is directly derived from the Taylor series expansion. For steadiness, the numerical dissipation should be introduced by different ways, such as using upwind schemes. However, a shortage of such schemes is that a long stencil is needed to achieve the desired order of accuracy, which makes the boundary schemes difficult to design [7]. To reduce the stencil width, the compact scheme becomes another choice. Compact FD schemes with spectral-like resolution are first systematically studied by Lele [8] and gain a quick development. Recently, Rizzetta et al. [5] carried out a high-order compact scheme with compact filter, which has been demonstrated to produce accurate and stable results in large eddy simulations. A family of hybrid dissipative compact schemes is proposed by Deng et al. [9] and suitable for simulations in aeroacoustics. To make compact schemes possess the shock-capturing capabilities, many efforts have been devoted [10–12], which were well summarized by Shen and Zha [13]. However, as stated by Tam [14], the Taylor series truncation cannot be used to quantity the wave propagation errors which are dominant in CAA and this issue results in the development of optimized schemes, where the order of accuracy is lowered to reduce errors over a range of wavenumbers [15]. One of the classical optimized schemes is the dispersion-relation-preserving (DRP) scheme developed by Tam and Webb [16], which is capable to accurately resolve harmonic components with few points-per-wavelength [17].

In most cases, the development of the FD schemes is based on the uniform Cartesian grids. However, in the simulations of practical problems, the use of the nonuniform or curvilinear grids is inevitable for adapting to the complex configurations. For solving this issue, some schemes are especially designed. Gamet et al. [18] modified the original compact scheme to approximate the first derivative on the nonuniform meshes. Cheong and Lee [19] developed the GODRP finite difference scheme to locally preserve the same dispersion relation as the original partial differential equations on the nonuniform mesh. Moreover, Zhong et al. [20,21] used the polynomial interpolation to derive arbitrary high-order compact schemes on nonuniform grids, which have been adopted for simulations of hypersonic boundary-layer stability and transition. Although these schemes can be directly applied on the nonuniform grids, the distribution of grids is still relatively simple (for example, the grids are only stretched along each direction of the Cartesian grids), making the schemes difficult to extend to practical conditions. Another method of dealing with the nonuniform or curvilinear grids in the FD schemes is to employ the coordinate transformation (or named Jacobian transformation), which is the most popular way. Using this method, the original schemes can be applied in the computational space where the grid is uniform Cartesian one, but as a result, the metrics and Jacobian are involved

https://doi.org/10.4208/aamm.2016.m1477 Published online by Cambridge University Press

in the governing equations, which should be carefully treated [22, 23].

At this moment, a problem arises naturally that when the coordinate transformation is introduced, whether the characteristics of the FD schemes that are evaluated on the uniform grids can be preserved, especially for the high-order schemes. The characteristics include the order of accuracy, resolution characteristics and the numerical stability. These characteristics are important for any numerical scheme and this problem is critical as we expect to apply the FD schemes to a wide range of flow simulations. Actually, many researchers have noticed this problem and carried out some studies. Gamet et al. [18] compared the calculation results based on the coordinate transformation with those using the nonuniform compact schemes on the random mesh. Visbal and Gaitonde [24] carried out detialed studies on the errors introduced by the mesh nonuniformities in finite-difference formulations. Chung and Tucker [25] compared the resolution characteristics by the Fourier analysis on uniform and nonuniform grids, but the detail expressions were not given. In this paper, we present a systematic analysis of the characteristics of the FD schemes in computing the first order spatial derivative on nonuniform grids, when the coordinate transformation is used. The nonuniformity involves many factors such as the grid size, stretching ratio and smoothness, which is a very complex problem. In this study, we restrict our attention to the smooth varying grids and the non-smooth case is left for further study. For the order of accuracy, we find that the designed order can be preserved, as the metrics are evaluated in the same high-order schemes. The resolution characteristics are studied by the Fourier analysis and we derive the dispersion and dissipation errors for the FD schemes when the metrics are included, which is not discussed before. The results show that the resolution characteristics on the nonuniform grids can be preserved as well, as long as the stretching ratio is controlled. The asymptotic stability is also analyzed by computing the eigenvalues of the matrices obtained by the spatial discretization. By comparison, it is found that the coordinate transformation may degrade the stability of the FD schemes when the stretch of grid is stronger at the boundary points, which puts forward higher requirements to the boundary schemes.

The rest of this paper is organized as follows. In the next section, we first present the one-dimensional wave equation after the coordinate transformation. Based on this equation, the order of accuracy, resolution characteristics and the asymptotic stability of the FD schemes on nonuniform grids are analyzed in Section 2.2 to Section 2.4. Numerical tests are presented in Section 3 to validate the analyses. Section 4 concludes this paper.

2 Analysis of the characteristics of the FD schemes on nonuniform grids

2.1 One-dimensional wave equation

In this section, the characteristics of the FD schemes when the coordinate transformation is used are analyzed in detail. These characteristics include the order of accuracy,

https://doi.org/10.4208/aamm.2016.m1477 Published online by Cambridge University Press

resolution characteristics and the numerical stability. For convenience, we take the one-dimensional wave equation into consideration,

$$\frac{\partial f}{\partial t}+a\frac{\partial f}{\partial x}=0. \tag{2.1}$$

Without loss of generality, we set a to be 1, so that the analytical solution of Eq. (2.1) is

$$f=g(x-t), \tag{2.2}$$

where the form of function g is determined by the initial conditions. As classified by Whitham [26], the solution represents a hypersonic wave with the constant phase speed and group velocity.

In numerical simulations, the first order spatial derivative is approximated by the numerical difference. In this paper, we discuss the effect of the coordinate transformation on the nonuniform grids, so Eq. (2.1) is transformed into

$$\frac{\partial f}{\partial t}+\xi_x\frac{\partial f}{\partial \xi}=0, \tag{2.3}$$

where ξ_x is the metric and satisfies $\xi_x=1/x_\xi$. As the coordinate transformation only influences the spatial derivative, the time integration is not discretized and keeps the analytical form in this study. Therefore, only the semi-discrete equation is used,

$$\frac{\partial f}{\partial t}+\left(\xi_x\delta^\xi f\right)_n=0, \tag{2.4}$$

where δ is the difference operator and the subscript n represents the position of the corresponding grid point.

2.2 The order of accuracy

For Eq. (2.4), the truncation errors are introduced by both the numerical difference and the evaluation of the metrics. After the transformation, the FD schemes in computing $\delta^\xi f$ are the same with those on uniform grids. In this paper, we adopt two FD schemes (COM6 and WCNS) that are developed by Lele [8] and Deng [11] respectively.

The compact scheme used by Lele is 6th-order and can be expressed as

$$\frac{1}{3}f'_{i-1}+f'_i+\frac{1}{3}f'_{i+1}=\frac{14}{9}\frac{f_{i+1}-f_{i-1}}{2\Delta\xi}+\frac{1}{9}\frac{f_{i+2}-f_{i-2}}{4\Delta\xi}, \tag{2.5}$$

where f' represents $\partial f/\partial\xi$ and $\Delta\xi$ is the interval in the computational space. In practice, the classical 4th-order Padé scheme and 3th-order compact relation are used for the non-periodic boundary problems [18] at points 2 and 1. The boundary formulations are

$$\frac{1}{4}f'_1+f'_2+\frac{1}{4}f'_3=\frac{3}{4\Delta\xi}(f_3-f_1), \tag{2.6a}$$

$$f'_1+2f'_2=\frac{1}{\Delta\xi}\left(-\frac{5}{2}f_1+2f_2+\frac{1}{2}f_3\right). \tag{2.6b}$$

https://doi.org/10.4208/aamm.2016.m1477 Published online by Cambridge University Press

Moreover, the explicit WCNS scheme based on the values at cell-edges is in the following form,

$$f_i' = \frac{75}{64\Delta\xi}(f_{i+1/2}-f_{i-1/2}) - \frac{25}{384\Delta\xi}(f_{i+3/2}-f_{i-3/2}) + \frac{3}{640\Delta\xi}(f_{i+5/2}-f_{i-5/2}), \tag{2.7}$$

which is also 6th-order. The values at cell-edges can be obtained by the interpolation and in consideration of the characteristic direction of Eq. (2.1), a 5th-order upwind interpolation is used,

$$f_{i+1/2} = \frac{3}{128}f_{i-2} - \frac{5}{32}f_{i-1} + \frac{45}{65}f_i + \frac{15}{32}f_{i+1} - \frac{5}{128}f_{i+2}. \tag{2.8}$$

The boundary schemes are discussed in [27]. The 5th-order interpolations at cell-edges $1/2$ and $3/2$ can be expressed as

$$f_{1/2} = \frac{1}{128}(315f_1 - 420f_2 + 378f_3 - 180f_4 + 35f_5), \tag{2.9a}$$

$$f_{3/2} = \frac{1}{128}(35f_1 + 140f_2 - 70f_3 + 28f_4 - 5f_5). \tag{2.9b}$$

The difference schemes at points 1 and 2 are

$$f_1{}' = \frac{1}{24}(-22f_{1/2} + 17f_{3/2} + 9f_{5/2} - 5f_{7/2} + f_{9/2}), \tag{2.10a}$$

$$f_2{}' = \frac{1}{24}(f_{1/2} - 27f_{3/2} + 27f_{5/2} - f_{7/2}), \tag{2.10b}$$

which are both 4th-order.

Besides the spatial derivative, the metrics should also be evaluated by the high-order numerical scheme to keep the overall order of accuracy. When the coordinate transformation is adopted in the FD schemes, another issue of the freestream preservation arises, which has been fully studied by many authors [22,23,28,29]. However, for Eq. (2.4), this issue is negligible and the metrics can be obtained in the same manner with the spatial derivative.

To study the effect of the coordinate transformation on the order of accuracy, Eq. (2.4) is solved. Numerical errors and the accuracy order are presented. The computational domain is $[-1,1]$ and the non-periodic boundary condition is specified at the left boundary. Two analytical solutions are used in this paper,

$$f(x,t) = \sin(-\pi x + \pi t - \pi), \tag{2.11a}$$

$$f(x,t) = \sin\left[\pi(x-t) - \frac{\sin[\pi(x-t)]}{\pi}\right]. \tag{2.11b}$$

Both the uniform and nonuniform grids are adopted and the stretching function proposed by Gamet [18] is used,

$$x_i = \eta_i + \frac{C-1}{\pi}\sin[\pi(\eta_i+1)] \quad \text{with} \quad -1 \le \eta_i = 2\frac{i-1}{N-1} - 1 \le +1, \tag{2.12}$$

https://doi.org/10.4208/aamm.2016.m1477 Published online by Cambridge University Press

Table 1: Numerical errors and the accuracy order on Eq. (2.11a).

	WCNS				COM6			
	Uniform grid		Nonuniform grid		Uniform grid		Nonuniform grid	
20	5.44088E-05	—	8.07521E-04	—	1.21289E-03	—	8.65392E-03	—
40	1.79230E-06	4.924	3.07065E-05	4.717	7.01554E-05	4.112	5.63927E-04	3.940
60	2.84135E-07	4.542	4.47558E-06	4.750	1.34682E-05	4.070	1.09116E-04	4.051
80	6.12175E-08	5.336	1.15817E-06	4.699	4.19476E-06	4.055	3.40422E-05	4.049
120	1.12671E-08	4.174	1.56420E-07	4.938	8.15535E-07	4.039	6.61649E-06	4.040

Table 2: Numerical errors and the accuracy order on Eq. (2.11b).

	WCNS				COM6			
	Uniform grid		Nonuniform grid		Uniform grid		Nonuniform grid	
20	5.44422E-04	—	2.45131E-03	—	2.93717E-03	—	1.56838E-02	—
40	1.72302E-05	4.982	9.05211E-05	4.759	1.55150E-04	4.242	1.03129E-03	3.992
60	2.36988E-06	4.893	1.33190E-05	4.726	2.91068E-05	4.127	1.19184E-04	5.322
80	5.58360E-07	5.025	3.34101E-06	4.807	9.00768E-06	4.077	5.92262E-05	2.431
120	7.57268E-08	4.927	4.81152E-07	4.779	1.74570E-06	4.047	1.14501E-05	4.053

where C is a constant and taken as $C=1.5$. The time advancement is accomplished through a 3th-order Runge-Kutta scheme and the time step is chosen to be small enough to make the errors in time negligible. Tables 1 and 2 present the errors and the accuracy order at $t=1$. It can be seen that although the absolute errors on the nonuniform grids are larger, nearly the same accuracy order is achieved on both the uniform and nonuniform grids. This shows that the designed accuracy order of the scheme can be preserved on nonuniform grids as the coordinate transformation is utilized in the FD method, as long as all terms in the equations are discretized in the corresponding high-order scheme.

2.3 Analysis of the resolution characteristics

The resolution characteristics of the FD schemes are analysed by the Fourier analysis, which is extensively described by Vichnevetsky and Bowles [30] and has become a classical technique for comparing differencing schemes [8]. However, most of the analyses are implemented on the uniform grids [31] or directly on the nonuniform grids [21]. The case that the coordinate transformation is involved is seldom studied. In this section, the detail formulae of the Fourier analysis of Eq. (2.3) are presented and the comparisons with the results on the uniform grids are made.

Following the discussions in [25], the mapping function between the uniform gird in the computational space ξ and the nonuniform grid in the physical space x is assumed to be

$$x=\frac{\sinh(\gamma\xi)}{\sinh(\gamma)}, \tag{2.13}$$

where γ is the control parameter and is set to be 3 in this paper. As the mapping function is known, we can use the analytical metrics in the discussion. For the compact scheme in

https://doi.org/10.4208/aamm.2016.m1477 Published online by Cambridge University Press

Eq. (2.5), the difference operator δ can be expressed in the matrix form,

$$\begin{bmatrix} \cdots & & & & \\ \alpha & 1 & \alpha & & \\ & \alpha & 1 & \alpha & \\ & & \alpha & 1 & \alpha \\ & & & & \cdots \end{bmatrix} \begin{bmatrix} \vdots \\ f'_{n-1} \\ f'_n \\ f'_{n+1} \\ \vdots \end{bmatrix} \tag{2.14}$$

$$= \begin{bmatrix} \cdots & & & & \\ -\frac{a}{2\Delta\xi} & 0 & \frac{a}{2\Delta\xi} & \frac{b}{4\Delta\xi} & \\ -\frac{b}{4\Delta\xi} & -\frac{a}{2\Delta\xi} & 0 & \frac{a}{2\Delta\xi} & \frac{b}{4\Delta\xi} \\ & -\frac{b}{4\Delta\xi} & -\frac{a}{2\Delta\xi} & 0 & \frac{a}{2\Delta\xi} \\ & & & & \cdots \end{bmatrix} \begin{bmatrix} \vdots \\ f_{n-1} \\ f_n \\ f_{n+1} \\ \vdots \end{bmatrix}, \tag{2.15}$$

where α, a and b are the coefficients in the FD scheme. The matrices at the LHS and RHS are defined as A_1 and A_2 respectively. Hence the semi-discrete equation Eq. (2.4) becomes

$$\frac{\partial}{\partial t} \begin{bmatrix} \vdots \\ f_{n-1} \\ f_n \\ f_{n+1} \\ \vdots \end{bmatrix} + \begin{bmatrix} \cdots & & & & \\ 0 & (\xi_x)_{n-1} & 0 & 0 & 0 \\ 0 & 0 & (\xi_x)_n & 0 & 0 \\ 0 & 0 & 0 & (\xi_x)_{n+1} & 0 \\ & & & & \cdots \end{bmatrix} A_1^{-1} A_2 \begin{bmatrix} \vdots \\ f_{n-1} \\ f_n \\ f_{n+1} \\ \vdots \end{bmatrix} = 0, \tag{2.16}$$

which can be further expressed as

$$\frac{\partial}{\partial t} A_1 \begin{bmatrix} \cdots & & & & \\ 0 & (\xi_x)_{n-1} & 0 & 0 & 0 \\ 0 & 0 & (\xi_x)_n & 0 & 0 \\ 0 & 0 & 0 & (\xi_x)_{n+1} & 0 \\ & & & & \cdots \end{bmatrix}^{-1} \begin{bmatrix} \vdots \\ f_{n-1} \\ f_n \\ f_{n+1} \\ \vdots \end{bmatrix} + A_2 \begin{bmatrix} \vdots \\ f_{n-1} \\ f_n \\ f_{n+1} \\ \vdots \end{bmatrix} = 0. \tag{2.17}$$

Taking any row in the above matrix, the semi-discrete equation can be written in another form,

$$\alpha \frac{1}{(\xi_x)_{n-1}} \frac{\partial f_{n-1}}{\partial t} + \frac{1}{(\xi_x)_n} \frac{\partial f_n}{\partial t} + \alpha \frac{1}{(\xi_x)_{n+1}} \frac{\partial f_{n+1}}{\partial t} + a \frac{f_{n+1} - f_{n-1}}{2\Delta\xi} + b \frac{f_{n+2} - f_{n-2}}{4\Delta\xi} = 0. \tag{2.18}$$

As $\xi_x = 1/x_\xi$, the above equation can be further simplified into

$$\alpha (x_\xi)_{n-1} \frac{\partial f_{n-1}}{\partial t} + (x_\xi)_n \frac{\partial f_n}{\partial t} + \alpha (x_\xi)_{n+1} \frac{\partial f_{n+1}}{\partial t} + a \frac{f_{n+1} - f_{n-1}}{2\Delta\xi} + b \frac{f_{n+2} - f_{n-2}}{4\Delta\xi} = 0, \tag{2.19}$$

https://doi.org/10.4208/aamm.2016.m1477 Published online by Cambridge University Press

which will be used in the Fourier analysis.

The essence of the Fourier analysis is to analyze the accuracy of the finite difference approximation of a partial differential equation [30]. Therefore the most straightforward method is to compare the analytical and approximate solutions. For Eq. (2.1), the analytical sinusoidal solution is in the form of

$$f(x,t)=v(0)e^{i\omega(x-t)}, \tag{2.20}$$

where ω is the space frequency (for the analytical solution of the wave equation, the time frequency Ω equals to ω) and $v(0)$ is defined by the initial condition. In the same manner, the approximate solution of the partial differential equation that is determined by Eq. (2.19) can be assumed in the following form,

$$p(\xi,\mathrm{t})=v(t)e^{i\omega\xi}, \tag{2.21}$$

where $v(t)=\tilde{v}(0)e^{\hat{A}(\omega)t}$ and $\tilde{v}(0)$ is also defined by the initial condition. As the approximate solution is obtained in the computational space, the independent variable in the function p is ξ, while ξ is a function of x. It is easy to verify that Eq. (2.21) is the solution of Eq. (2.19), as long as $\hat{A}(\omega)$ satisfies

$$\hat{A}(\omega)=-\frac{\frac{b}{4\triangle\xi}e^{i\omega\xi_{n+2}}+\frac{a}{2\triangle\xi}e^{i\omega\xi_{n+1}}-\frac{a}{2\triangle\xi}e^{i\omega\xi_{n-1}}-\frac{b}{4\triangle\xi}e^{i\omega\xi_{n-2}}}{\alpha\left(x_\xi\right)_{n-1}e^{i\omega\xi_{n-1}}+\left(x_\xi\right)_n e^{i\omega\xi_n}+\alpha\left(x_\xi\right)_{n+1}e^{i\omega\xi_{n+1}}}. \tag{2.22}$$

Substituting it into Eq. (2.21) leads to

$$p(\xi,t)=\tilde{v}(0)e^{\hat{A}(\omega)t}e^{i\omega\xi}=\tilde{v}(0)e^{Re\left[\hat{A}(\omega)\right]t}e^{i\left(\omega\xi+Im\left[\hat{A}(\omega)\right]t\right)}. \tag{2.23}$$

$Re\left[\hat{A}(\omega)\right]$ and $Im\left[\hat{A}(\omega)\right]$ represent the real part and the imaginary part of $\hat{A}(\omega)$, which correspond to the dissipative and dispersive errors respectively. $\hat{A}(\omega)$ can be further simplified into

$$\begin{aligned}&\hat{A}(\omega)\\&=-\frac{\left[\frac{b}{2\Delta\xi}\sin(2\omega\Delta\xi)+\frac{a}{\Delta\xi}\sin(\omega\Delta\xi)\right]i}{\left[\alpha\left(x_\xi\right)_{n-1}\cos(\omega\Delta\xi)+\left(x_\xi\right)_n+\alpha\left(x_\xi\right)_{n+1}\cos(\omega\Delta\xi)\right]+\left[\alpha\left(x_\xi\right)_{n+1}\sin(\omega\Delta\xi)-\alpha\left(x_\xi\right)_{n-1}\sin(\omega\Delta\xi)\right]i},\end{aligned} \tag{2.24}$$

from which it is found that it is the metrics that make sense in the Fourier analysis, not the coordinates of grid points. As the distribution of the grid points in space ξ is uniform, x_ξ reflects the stretching ratio of the grid points in the physical space, which is widely used and controlled in grid generations. Therefore the effect of the nonuniform grids on the resolution characteristics is evaluated by the stretching ratio in this paper, instead of the coordinates of grid points.

Based on above equations, the dissipation errors of the FD schemes are evaluated by the real part of $\hat{A}(\omega)$, which is zero for the analytical solution. The dispersive errors are

https://doi.org/10.4208/aamm.2016.m1477 Published online by Cambridge University Press

related to the imaginary part of $\hat{A}(\omega)$. In order to express the dispersive errors in an intuitive way, we first calculate the phase velocity of Eq. (2.23),

$$c^* = -\left(x_\xi\right)_n \frac{Im\left[\hat{A}(\omega)\right]}{\omega}. \tag{2.25}$$

As the phase velocity is different as the spatial position changes, the value of the metric in Eq. (2.25) is obtained at the calculation grid point n. The exact phase velocity of the wave equation is $c^* = 1$, so that the dispersive errors can be evaluated by comparing the phase velocity, which is often depicted in the figure of time frequency Ω and space frequency ω [30],

$$\Omega = \omega c^*(\omega). \tag{2.26}$$

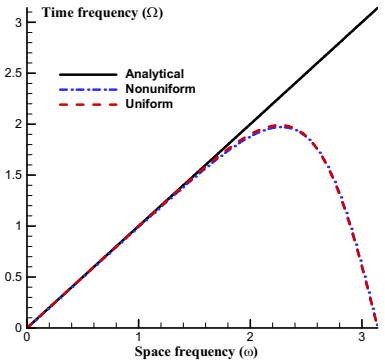
In Eq. (2.26), the analytical metrics are used and the influence of the nonuniform grids are evaluated by the stretching ratio, which is defined as

$$r = \frac{x_{n+1} - x_n}{x_n - x_{n-1}}. \tag{2.27}$$

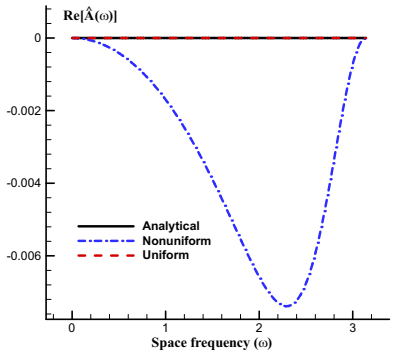
For Eq. (2.13), the computational domain in the physical space is $[1,2]$ and the stretching ratio is controlled by adding or removing grid points. The results on the uniform grids can be easily obtained by setting the metrics to be constant. Fig. 1 shows the dissipative and dispersive errors with different stretching ratios. Moreover, results on the uniform grids and the exact solution are presented at the same time. It can be observed from Fig. 1 that although the symmetry schemes are designed to be non-dissipative on the uniform grids, the dissipative errors are non-zero on the nonuniform grids. As the stretching ratio increases, more dissipative errors are introduced in the numerical scheme. Dispersive errors are also greatly influenced by the stretching ratio: if it is small, the difference of dispersive errors between the uniform and nonuniform grids is indistinguishable; however, if amplified, the dispersive errors on the nonuniform grids experience an obvious increase, and degrade the resolution characteristics.

The above discussions are based on the compact scheme (COM6). For the explicit one, it is just a special case of the compact scheme with $\alpha = 0$. Substitute it into Eqs. (2.24) and (2.25) and it is easy to verify that the dissipative and dispersive errors are the same with those on the uniform grids. This is because the metric used in Eq. (2.25) is obtained at the calculation grid point n, which will be divided out by the metric in Eq. (2.24). Therefore $\hat{A}(\omega)$ becomes a pure imaginary number and brings in no dissipation error. However, different from the consistent resolution characteristics on the uniform grids, the dispersive errors vary in space on the nonuniform grids. To further study the effect of the stretching ratio on the explicit scheme, we present the dispersive errors at the half points on the left and right of the calculation point. Accordingly, the metrics in Eq. (2.25) are replaced by $\left(x_\xi\right)_{n-1/2}$ and $\left(x_\xi\right)_{n+1/2}$. For convenience, we use a 4th-order explicit scheme with $\alpha = 0$, $a = 4/3$ and $b = -1/3$. The dispersion errors for different stretching

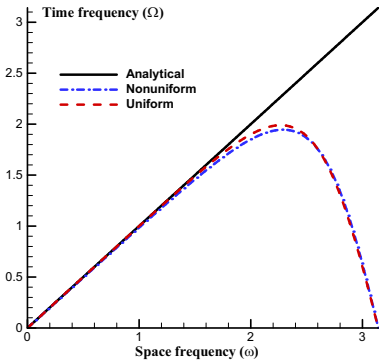
https://doi.org/10.4208/aamm.2016.m1477 Published online by Cambridge University Press



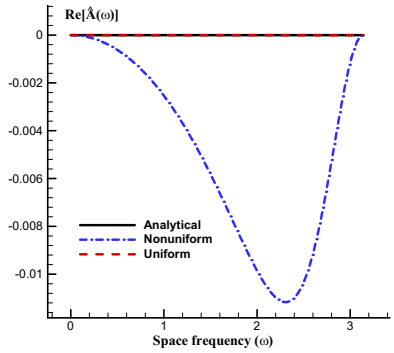
(a) Dispersive errors with $r=1.15$



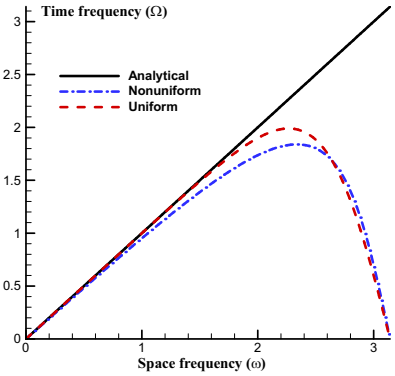
(b) Dissipative errors with $r=1.15$



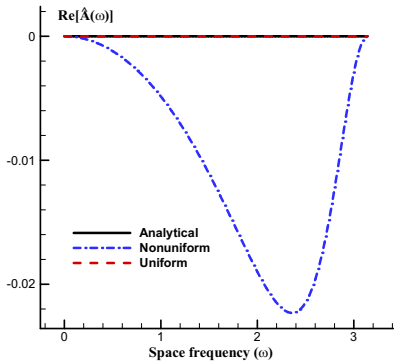
(c) Dispersive errors with $r=1.25$



(d) Dissipative errors with $r=1.25$



(e) Dispersive errors with $r=1.50$



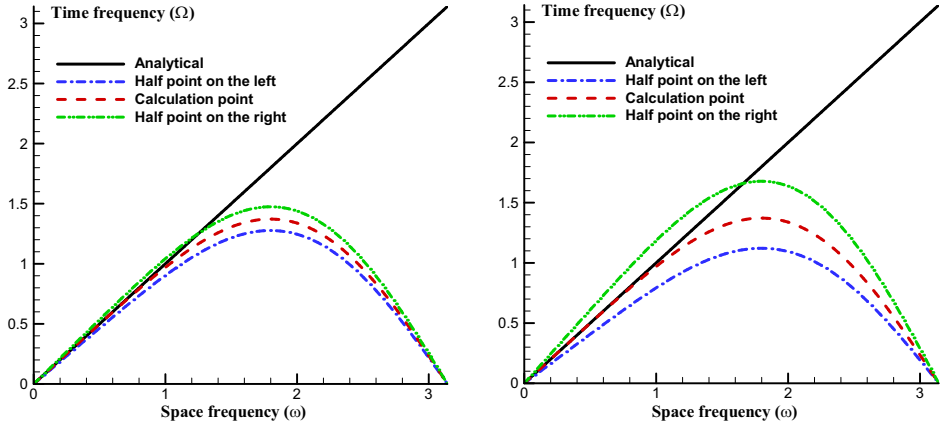
(f) Dissipative errors with $r=1.50$

Figure 1: The dispersive and dissipative errors for different stretching ratios.

ratios are shown in Fig. 2. Similar with the results in the compact scheme, the dispersion errors are enlarged rapidly and become unacceptable as the stretching ratio increases.

From the above discussions, it is found that the resolution characteristics of the FD

https://doi.org/10.4208/aamm.2016.m1477 Published online by Cambridge University Press



(a) $r=1.15$ (b) $r=1.50$

Figure 2: The dispersive errors for different stretching ratios at the calculation point and the half points on its left and right.

schemes have a close relation with the stretching ratio of the grids. The characteristics can be preserved as long as the stretching ratio is controlled, no matter for the compact or explicit schemes. Actually, in the practical process of grid generations, the stretching ratio is often required to be less than 1.25. The current study also validates the requirement from the resolution characteristics point of view.

2.4 Asymptotic stability analysis

The asymptotic stability is an important characteristic of the numerical schemes and it decides whether a scheme can be used for solving Eq. (2.1). Carpenter et al. [32] started an early discussion about this issue. Based on the semi-discrete equation, the first-order spatial derivative at all grid points including interior and the boundary can be written as

$$[M_1]\{f'\}=[M_2]\{f\}. \tag{2.28}$$

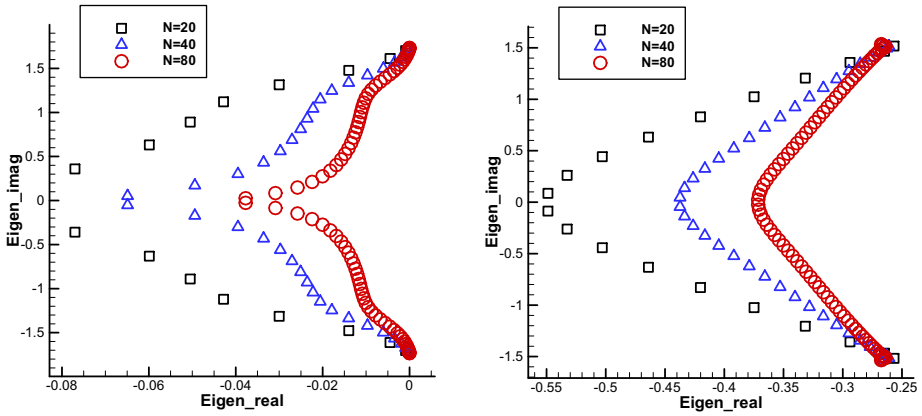
Substituting the above equation into Eq. (2.1) leads to

$$\left\{\frac{df}{dt}\right\}=[M]\{f\}+\{g(t)\}, \tag{2.29}$$

where $[M]=-[M_1]^{-1}[M_2]$, and $g(t)$ represents the physical boundary conditions imposed on the boundary grid point. If the coordinate transformation is used, the metrics are introduced and Eq. (2.29) becomes

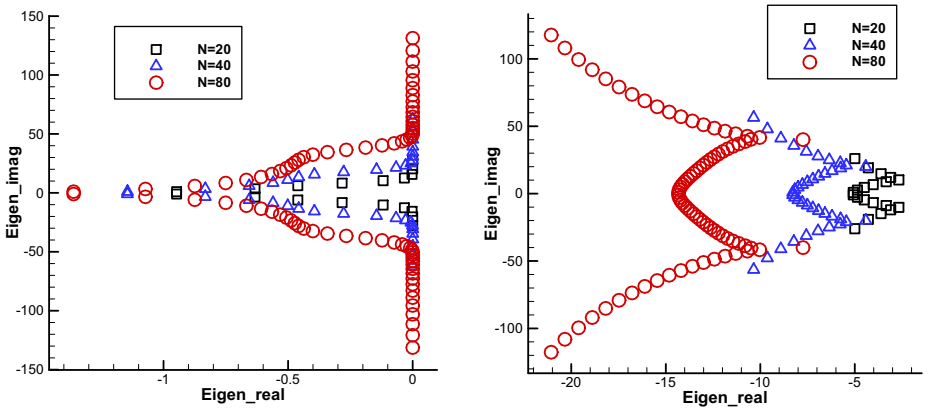
$$\left\{\frac{df}{dt}\right\}=[D]^{-1}[M]\{f\}+\{g'(t)\}, \tag{2.30}$$

https://doi.org/10.4208/aamm.2016.m1477 Published online by Cambridge University Press



(a) COM6 (b) WCNS

Figure 3: The eigenvalue spectra of COM6 and WCNS schemes on the uniform grid.



(a) COM6 (b) WCNS

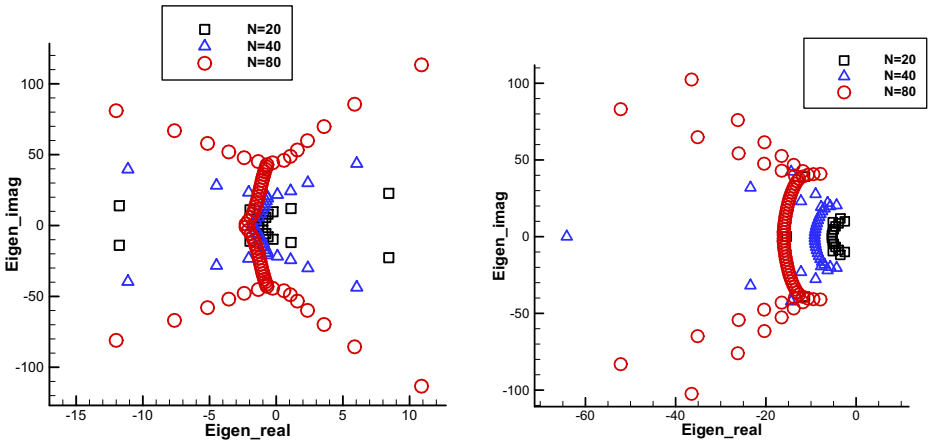
Figure 4: The eigenvalue spectra of COM6 and WCNS schemes on the nonuniform grid defined by Eq. (2.12).

where $[D]$ is a diagonal matrix such that

$$diag[D]=[(\xi_x)_i],\quad i=1,\cdots,N. \tag{2.31}$$

For guaranteeing the stability of the overall FD schemes, it is required that the eigenvalues of Eq. (2.30) lie in the left half of the complex plane. In this section, we first present the asymptotic stability analysis on the uniform grids. The eigenvalue spectra of COM6 and WCNS schemes is shown in Fig. 3. It can be seen that all the eigenvalues are in the left half and both schemes are steady. For the nonuniform grids, the coordinate transformation is introduced and the characteristic of the eigenvalues has a close relation with the grid distribution. Fig. 4 presents the eigenvalue spectra on the nonuniform grid defined by Eq. (2.12). On this grid, both schemes are steady, which is also demonstrated

https://doi.org/10.4208/aamm.2016.m1477 Published online by Cambridge University Press



(a) COM6 (b) WCNS

Figure 5: The eigenvalue spectra of COM6 and WCNS schemes on the nonuniform grid defined by Eq. (2.32).

by the practical calculations in Section 2.2. In order to further study the behavior of the eigenvalues on the nonuniform grids, another spacing function with strong stretch is used [33],

$$x_i = \frac{\sin^{-1}[-\alpha\cos(\pi i/N)]}{\sin^{-1}\alpha}, \quad i=0,\cdots,N, \tag{2.32}$$

where α controls the grid points from a Chebyshev grid ($\alpha \to 0$) to a uniform grid ($\alpha = 0$). In this paper, α is chosen to be 0.5 and Fig. 5 presents the eigenvalue spectra. Fig. 5 shows that the WCNS scheme is still steady on this grid, but the real part of the eigenvalues gets close to zero. On the other hand, the COM6 scheme becomes unsteady as some eigenvalues appear in the right half of the complex plane. This is because the stretch is stronger at the boundary points where the boundary schemes are implemented.

Actually, the design of steady boundary schemes is a challenge for the high-order schemes in the FD method. The above discussions indicate that the nonuniform grids may aggravate this problem, especially when the strong stretch exists at boundary points. However this condition is usually encountered in solving the Euler or Navier-Stokes equations. Therefore the development of steady boundary schemes in the high-order FD method is critical. Furthermore, it should be noted that the asymptotic stability analysis is based on the linear wave equation, which cannot fully represent the characteristics of the numerical schemes in solving nonlinear equations. This may leave us the possibility to obtain the high-order and steady boundary schemes.

From the above analysis in Sections 2.2 to 2.4, we find that the characteristics of the FD schemes can be generally preserved on the nonuniform grids when the coordinate transformation is used. However, the discussions are based on the smooth varying nonuniform grids. The cases of non-smooth or random grids are out of the scope of this paper.

https://doi.org/10.4208/aamm.2016.m1477 Published online by Cambridge University Press

3 Numerical results

In this section, numerical tests are presented to validate the analyses in this paper. In consideration of the good numerical stability, the 5th-order explicit WCNS scheme is used. Although the second spatial derivative corresponding to the viscous terms is not discussed, a test case governed by the Navier-Stokes equations is also included. The numerical schemes for the viscous terms can be found in [34] for detail. In multi-dimensional problems, the metrics and Jacobian are evaluated by the symmetric conservative metric method (SCMM) developed by Deng [23].

3.1 Two-dimensional channel flow

The two-dimensional channel flow is an isentropic flow governed by the Euler equations, which was first discussed by Casper et al. [35]. In this paper, the C3 geometry is used, and the shape of the middle section is determined by

$$\begin{cases} y_1(x)=-0.5+0.05\sin^4\left(\dfrac{10}{9}\pi x+\dfrac{\pi}{2}\right), \\ y_2(x)=0.5-0.05\sin^4\left(\dfrac{10}{9}\pi x+\dfrac{\pi}{2}\right), \end{cases} \tag{3.1}$$

where $y_1(x)$ and $y_2(x)$ represent the lower and upper walls respectively. Other parts of the walls are alone the direction of x and defined by

$$\begin{cases} y_1(x)=-0.5, \\ y_2(x)=0.5. \end{cases} \tag{3.2}$$

The grid is generated by a mapping from a rectangle space (ξ,η) to the physical point (x,y),

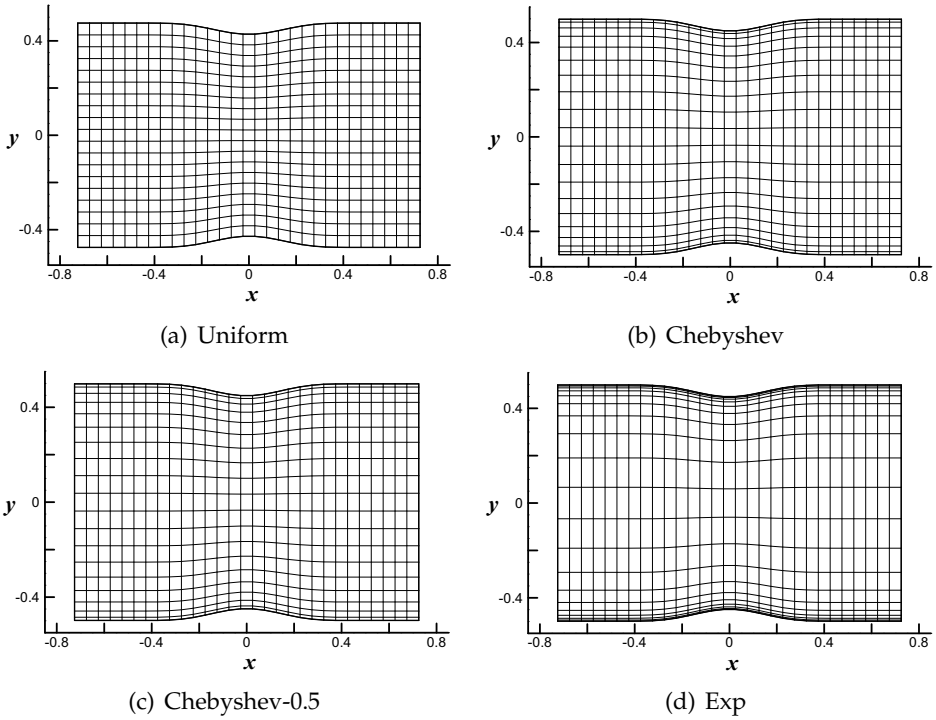
$$\begin{cases} x=\xi, \\ y=\left(1-\dfrac{\eta}{H}\right)y_1(\xi)+\dfrac{\eta}{H}y_2(\xi). \end{cases} \tag{3.3}$$

Moreover, the boundary conditions used in this test case are presented in [36].

To demonstrate that the FD schemes after the coordinate transformation can preserve the original characteristics, four different grids are used in the numerical calculations, which are labeled as Uniform, Chebyshev, Chebyshev-0.5 and Exp. The Uniform grid does not mean the grid in the physical space is uniform, but the gird in the rectangle space (ξ,η) is uniform and the other grids are defined in the same manner. The Chebyshev represents a Chebyshev grid alone η and the Chebyshev-0.5 defines the grid by Eq. (2.32) with $\alpha=0.5$. The grid labeled as Exp is generated by the following mapping function,

$$\eta(\varphi)=\frac{A(\beta+2\gamma)+2\gamma-\beta}{(2\gamma+1)(1+A)}, \qquad A=\left(\frac{\beta+1}{\beta-1}\right)^{(1-\varphi-\gamma)/(\gamma-1)}, \tag{3.4}$$

https://doi.org/10.4208/aamm.2016.m1477 Published online by Cambridge University Press



(a) Uniform (b) Chebyshev

(c) Chebyshev-0.5 (d) Exp

Figure 6: The configuration of the two-dimensional channel and different grids used in the calculations.

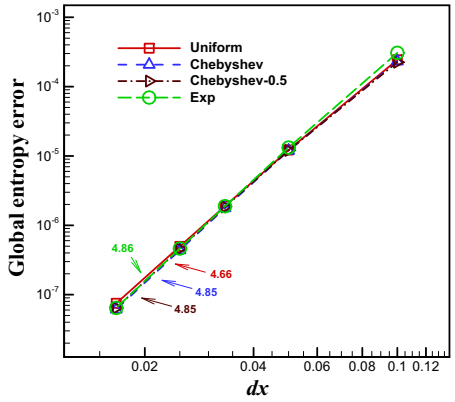


Figure 7: Global entropy errors in the two-dimensional channel flow on different grids.

where $\gamma = 0.5$ and $\beta = 1.01015$ are constant [37]. Fig. 6 illustrates the configuration of the channel and different grids.

The global L_1 entropy errors on different grids are listed in Table 3 and also plotted in Fig. 7. It can be seen that the entropy errors agree well with each other and the

https://doi.org/10.4208/aamm.2016.m1477 Published online by Cambridge University Press

Table 3: Global L_1 entropy errors on different grids.

Grid	Uniform	Chebyshev	Chebyshev-0.5	Exp
15×10	2.4369E-04	2.3247E-04	2.2515E-04	3.0725E-04
30×20	1.2189E-05	1.1906E-05	1.2034E-05	1.3227E-05
45×30	1.8928E-06	1.7744E-06	1.8408E-06	1.8853E-06
60×40	4.9728E-07	4.3888E-07	4.6006E-07	4.6299E-07
90×60	7.5057E-08	6.1315E-08	6.4355E-08	6.4433E-08

distribution of the grid points does not influence the numerical results much. The calculated order of accuracy is presented in Fig. 7 as well, and all the values are close to 5.0. It indicates that the designed accuracy order can be preserved when the coordinate transformation is used and this technique is indeed usable in the practical simulations.

3.2 Two-dimensional isentropic vortex

This problem is widely used in testing a high-order CFD method's capacity to preserve vorticity in an unsteady inviscid flow [38]. The initial flow is the superposition of a uniform flow and a vortical movement. As periodic boundary conditions are adopted, the analytical solution after several periods euqals to the initial state. Therefore the errors introduced by the numerical schemes can be easily evaluated. The distribution of the velocity can be expressed as

$$\begin{cases} u_0 = U_\infty - (U_\infty \beta)\dfrac{y-Y_c}{R}\exp\left(-\dfrac{r^2}{2}\right), \\ v_0 = (U_\infty \beta)\dfrac{x-X_c}{R}\exp\left(-\dfrac{r^2}{2}\right), \end{cases} \tag{3.5}$$

where $r=\frac{\sqrt{(x-X_c)^2+(y-Y_c)^2}}{R}$ and U_∞ is the unperturbed velocity. The calculation of the pressure, temperature and density can be found in [38]. In this paper, the computational domain is $(x,y)\in[0,L_x]\times[0,L_y]$ and L_x=0.1, L_y=0.1. The center of the vortex is at X_c=0.05, $Y_c=0.05$ and the initial pressure and temperature are $p_\infty=10^5$Pa and $T_\infty=300$K. Mach number Ma=0.05 is chosen with β=0.02 and R=0.005. Because the vortex is transported by a uniform flow, we define the period T as $T=L_x/U_\infty$ and the errors of the velocity u are collected after 50 periods.

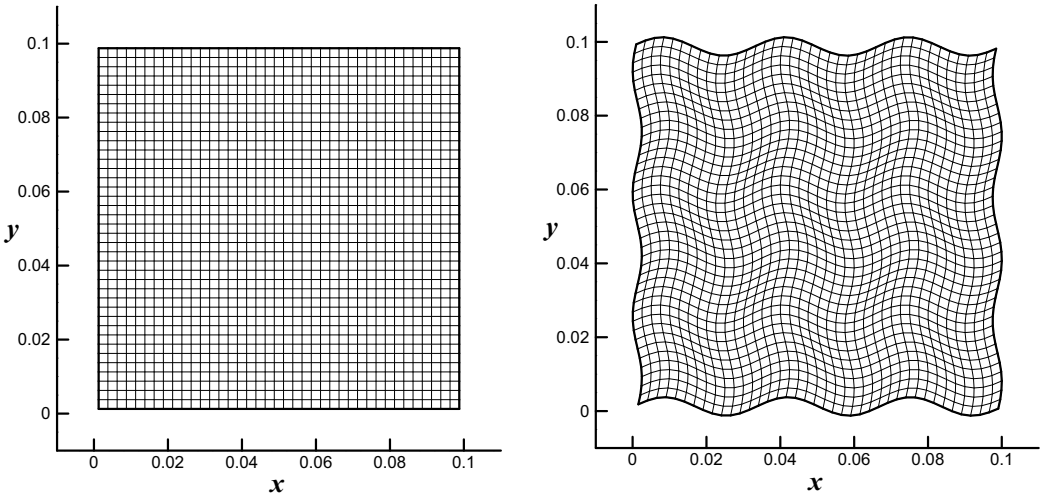
Two kinds of girds are used in this test case, which are the uniform grid and the wavy grid respectively. The wavy grid is generated by the following formula [24],

$$x_{i,j} = x_{\min} + \Delta x_o\left[(i-1)+\sin\left(\frac{6\pi(j-1)\Delta y_o}{L_y}\right)\right], \tag{3.6a}$$

$$y_{i,j} = y_{\min} + \Delta y_o\left[(j-1)+2\sin\left(\frac{6\pi(i-1)\Delta x_o}{L_x}\right)\right], \tag{3.6b}$$

(3.6c)

https://doi.org/10.4208/aamm.2016.m1477 Published online by Cambridge University Press



(a) Uniform grid (b) Wavy grid

Figure 8: The uniform and wavy grids used in the problem of two-dimensional isentropic vortex.

$$\Delta x_o = \frac{L_x}{IL-1}, \quad \Delta y_o = \frac{L_y}{JL-1}, \quad 1 \le i \le IL, \quad 1 \le j \le JL, \tag{3.6d}$$

where IL and JL denote the number of points in the ξ and η directions and $x_{\min}=y_{\min}=0$. Both girds are shown in Fig. 8. Table 4 presents the errors of u and the accuracy order with different grid numbers. It can be seen that the designed order of the scheme is both achieved. The abnormality of the order between the first two girds is due to relatively stronger dissipation on coarse grids, which causes problems in the error statistics. Fig. 9 shows the numerical results with the grid number 120×120. In Fig. 9(a), the value of u alone the vertical centerline is plotted. The numerical result on the wavy grid deviates the analytical solution more than that on the uniform grid. This indicates that the scheme introduces more dissipation errors on the wavy grid. Figs. 9(b) and 9(c) compare the vorticity magnitude contours. Some nonphysical wiggles are observed on the wavy grid, due to the dispersive errors. As we know, in this test case, the best results are obtained on the uniform Cartesian grids. However, from the above comparisons, we find the

Table 4: Numerical errors and accuracy order of u with different grid number at $t=50T$.

Grid	Uniform grid		Wavy grid	
40×40	3.59861E-04	—	3.83602E-04	—
80×80	1.19638E-04	1.589	2.30041E-04	0.738
120×120	3.18750E-05	3.262	6.06152E-05	3.289
160×160	9.21134E-06	4.315	1.44412E-05	4.986
240×240	1.30105E-06	4.827	1.68295E-06	4.779

https://doi.org/10.4208/aamm.2016.m1477 Published online by Cambridge University Press

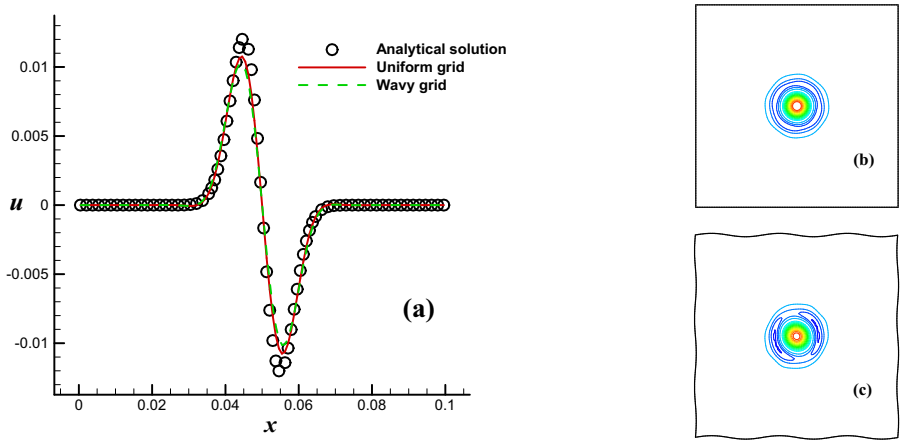


Figure 9: Numerical results on the uniform and wavy grids with grid number 120×120. (a) u alone the vertical centerline. (b) Vorticity magnitude contours on uniform grid. (c) Vorticity magnitude contours on wavy grid.

results on the wavy mesh are equally acceptable. The flowfield is well preserved when the coordinate transformation is used in the FD method.

3.3 Laminar flow around a delta wing

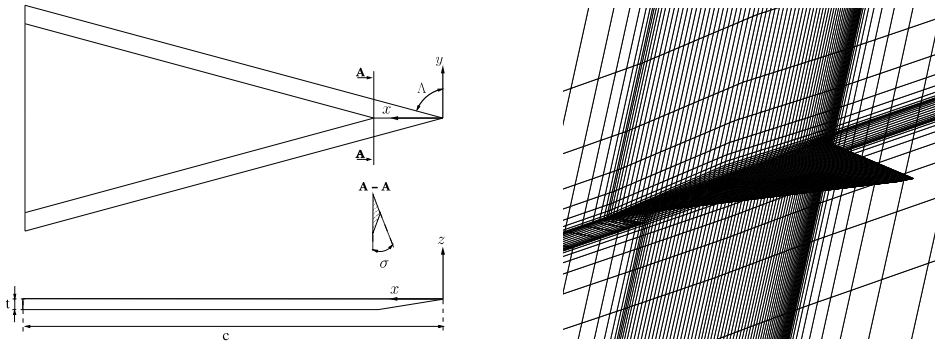
This test case is designed in the EU project ADIGMA [40]. With a free stream Mach number $Ma=0.5$, Reynolds number $\mathrm{Re}=4000$ and at an angle of $\alpha=12.5^\circ$, the delta wing is considered at the laminar conditions. As the flow passes the leading edge, it rolls up and creates a large vortex and a secondary vortex which are convected far behind the wing.

The geometry of delta wing [39] and a coarse grid are presented in Fig. 10. In this paper, three different grids labeled as coarse, medium and fine are used in simulations and the grid number is increased by the ratio of 8. Because of the complex structure of the grids, the coordinate transformation should be used. The solution is initialized by a uniform flow and the no-slip adiabatic wall boundary condition is imposed. For comparison, both the 2nd-order and 5th-order schemes are adopted in this paper and all the calculations can converge to the machine zero. Table 5 collects the lift and drag coeffi-

Table 5: Lift and drag coefficients of the delta wing on three grids.

	Coarse	Medium	Fine	Referance [41]
Lift coefficient (5th order)	0.362	0.355	0.352	0.347
Drag coefficient (5th order)	0.1715	0.1700	0.1675	0.1658
Lift coefficient (2th order)	0.373	0.357	0.351	0.347
Drag coefficient (2th order)	0.1759	0.1700	0.1682	0.1658

https://doi.org/10.4208/aamm.2016.m1477 Published online by Cambridge University Press



(a) Geometry of the delta wing [39] with $\Lambda=75^\circ$, $\sigma=60^\circ$, $t/c=0.024$.

(b) The constructed grid used in the simulation.

Figure 10: The configuration and grid of the delta wing.

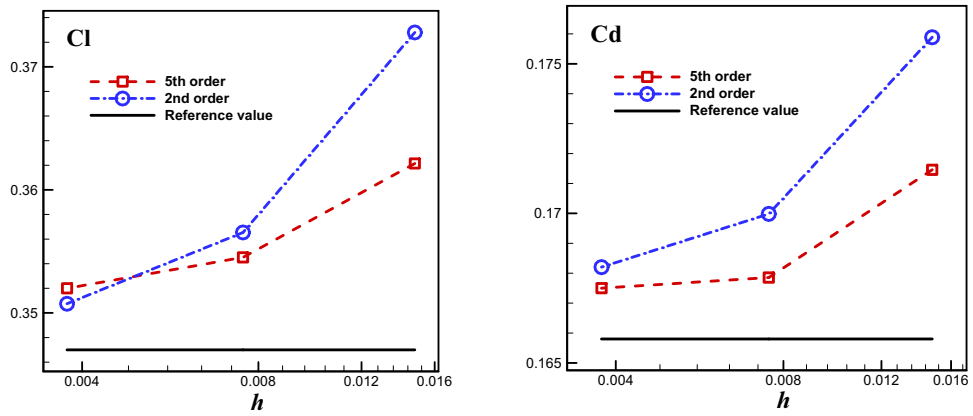


Figure 11: Lift (left) and drag (right) coefficients of using 5th-order and 2nd-order schemes with different grid sizes.

cients on three grids. For reference, the values of extrapolating the results obtained with a higher order DG method [41] are included. Fig. 11 shows the lift and drag coefficients with different grid sizes. It can be seen that as the grid is refined, the lift and drag coefficients both converge to the reference values, but the high-order scheme has a more rapid rate. The benefit of using a high-order scheme in the numerical calculations is obvious, as the vortex structure over the wing can be better captured. This test case demonstrates the schemes used in this paper can well resolve the features of the flowfield and can be applied in the simulations of practical problems.

In addition, the Mach number contours at $x=2.6c$ for both the 2nd-order and 5th-order schemes are presented in Fig. 12. From the comparison, it is found that the secondary vortex can be well captured using the 5th-order scheme, while the 2nd-order scheme has a much worse resolution. The advantage of the high-order scheme is ob-

https://doi.org/10.4208/aamm.2016.m1477 Published online by Cambridge University Press

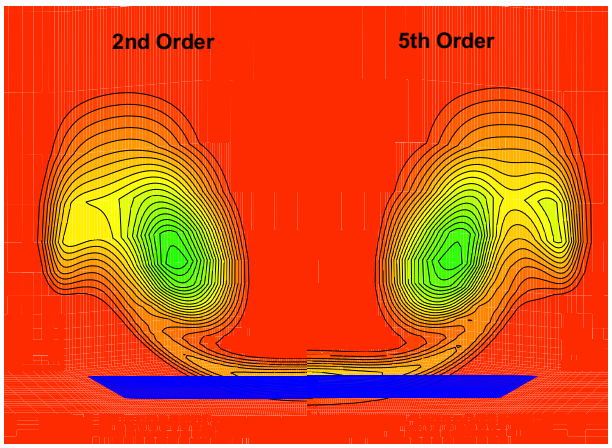


Figure 12: Comparison of the Mach number contours of the 2nd-order and 5th-order schemes at $x=2.6c$.

vious in this test case. In [25], the authors pointed out that as the grid nonuniformity increased, if the coordinate transformation was used, the benefit of using higher-order schemes would almost disappear. However, from the results obtained in this paper, we consider this conclusion may be worth discussing.

4 Conclusions

In this paper, systematical studies of the characteristics of the FD schemes on nonuniform grids when the coordinate transformation is introduced are carried out. Focused on the smooth varying grids, detail analyses are presented and can be summarized as follows:

(i) For the order of accuracy, the designed order of the schemes can be preserved on the nonuniform grids. The accuracy deterioration in higher-order FD schemes described in [25] is not found.

(ii) Formulae of the Fourier analysis involving the coordinate transformation are presented for the first time. Based on the current method, it is found that the resolution characteristics of the FD schemes on nonuniform grids have a close relation with the stretching ratio of grids. The resolution characteristics can be preserved as well, as long as the stretching ratio is reasonably controlled.

(iii) Asymptotic stability analysis shows that the coordinate transformation may degrade the stability of some FD schemes, which is closely related to the boundary schemes. This issue deserves more attention.

In general, the characteristics of the FD schemes can be preserved after the coordinate transformation, which is also demonstrated by numerical tests.

https://doi.org/10.4208/aamm.2016.m1477 Published online by Cambridge University Press

In the current paper, we only analyze the behaviors of first spatial derivative that represents the calculations of the convective terms. In fact, the viscous terms are equally important and worth studying. The effect of non-smooth girds on the FD schemes is a big and complex topic. Quantitative analysis is seldom seen. These issues are of great importance in the development of the FD method and we expect further studies.

Acknowledgments

This work was supported by the Basic Research Foundation of National University of Defense Technology (No. ZDYYJCYJ20140101). We are very grateful to the referees of this paper for their valuable suggestions to improve the quality of this paper.

References

[1] M. VINOKUR, *An analysis of finite-difference and finite-volume formulations of conservation laws*, J. Comput. Phys., 81 (1989), pp. 1–52.
[2] D. J. GARMANN, *Compact finite-differencing and filtering procedure applied to the incompressible navier-stokes equations*, AIAA J., 51(9) (2013).
[3] X. ZHANG AND C. W. SHU, *Positivity-preserving high order finite difference WENO schemes for compressible Euler equations*, J. Comput. Phys., 231 (2012), pp. 2245–2258.
[4] O. MARXEN, G. IACCARINO AND T. E. MAGIN, *Direct numerical simulations of hypersonic boundary-layer transition with finite-rate chemistry*, J. Fluid Mech., 755 (2014), pp. 35–49.
[5] D. P. RIZZETTA, M. R. VISBAL AND P. E. MORGAN, *A high-order compact finite-difference scheme for large-eddy simulation of active flow control*, Progress Aerospace Sci., 44 (2008), pp. 397–426.
[6] Y. MOR-YOSSEF, *Unconditionally stable time marching scheme for reynolds stress models*, J. Comput. Phys., 276 (2014), pp. 635–664.
[7] J. A. EKATERINARIS, *High-order accurate, low numerical diffusion methods for aerodynamics*, Progress Aerospace Sci., 41 (2005), pp. 192–300.
[8] S. K. LELE, *Compact finite difference schemes with spectral-like resolution*, J. Comput. Phys., 103 (1992), pp. 16–42.
[9] X. DENG, Y. JIANG, M. MAO, H. LIU, S. LI AND G. TU, *A family of hybrid cell-edge and cell-node dissipative compact schemes satisfying geometric conservation law*, Comput. Fluids, 116 (2015), pp. 29–45.
[10] B. COCKBURN AND C. W. SHU, *Nonlinearly stable copact schemes for shock calculations*, SIAM J. Numer. Anal., 31(3) (1994), pp. 607–627.
[11] X. DENG AND H. MAEKAWA, *Compact high-order accurate nonlinear schemes*, J. Comput. Phys., 130 (1997), pp. 77–91.
[12] Y.-X. REN, M. LIU AND H. ZHANG, *A characteristic-wise hybrid compact-WENO scheme for solving hyperbolic conservation laws*, J. Comput. Phys., 192 (2003), pp. 365–386.
[13] Y. SHEN AND G. ZHA, *Generalized finite compact difference scheme for shock/complex flowfield interaction*, J. Comput. Phys., 230 (2011), pp. 4419–4436.
[14] C. K. W. TAM, Computational Aeroacoustics: A Wave Number Approach, Cambridge University Press, 2012.

https://doi.org/10.4208/aamm.2016.m1477 Published online by Cambridge University Press

[15] D. W. ZINGG, S. D. RANGO, M. NEMEC AND T. H. PULLIAM, *Comparison of several spatial discretizations for the Navier–Stokes equations*, J. Comput. Phys., 160 (2000), pp. 683–704.
[16] C. K. W. TAM AND J. C. WEBB, *Dispersion-relation-preserving finite difference schemes for computational acoustics*, J. Comput. Phys., 107 (1993), pp. 262–281.
[17] S. PIROZZOLI, *Performance analysis and optimization of finite-difference schemes for wave propagation problems*, J. Comput. Phys., 222 (2007), pp. 809–831.
[18] L. GAMET, F. DUCROS, F. NICOUD AND T. POINSOT, *Compact finite difference schemes on non-uniform meshes, application to direct numerical simulations of compressible flows*, Int. J. Numer. Meth. Fluids, 29 (1999), pp. 159–191.
[19] C. CHEONG AND S. LEE, *Grid-optimized dispersion-relation-preserving schemes on general geometries for computational aeroacoustics*, J. Comput. Phys., 174 (2001), pp. 248–276.
[20] X. ZHONG AND M. TATINENI, *High-order non-uniform grid schemes for numerical simulation of hypersonic boundary-layer stability and transition*, J. Comput. Phys., 190 (2003), pp. 419–458.
[21] R. K. SHUKLA AND X. ZHONG, *Derivation of high-order compact finite difference schemes for non-uniform grid using polynomial interpolation*, J. Comput. Phys., 204 (2005), pp. 404–429.
[22] X. DENG, M. MAO, G. TU, H. LIU AND H. ZHANG, *Geometric conservation law and application to high-order finite difference schemes with stationary grids*, J. Comput. Phys., 230 (2011), pp. 1100–1115.
[23] X. DENG, Y. MIN, M. MAO, H. LIU, G. TU AND H. ZHANG, *Further study on geometric conservation law and application to high-order finite difference schemes with stationary grids*, J. Comput. Phys., 239 (2013), pp. 90–111.
[24] R. VISBAL AND D. GAITONDE, *On the use of higher-order finite-difference schemes on curvilinear and deforming meshes*, J. Comput. Phys., 181 (2002), pp. 155–185.
[25] Y. M. CHUNG AND P. G. TUCKER, *Accuracy of higher-order finite difference schemes on nonuniform grids*, AIAA J., 41(8) (2003).
[26] G. B. WHITHAM, Linear and Nonlinear Waves, John Wiley & Sons, 1974.
[27] X. DENG AND H. ZHANG, *Developing high-order weighted compact nonlinear schemes*, J. Comput. Phys., 165 (2000), pp. 22–44.
[28] M. VINOKUR AND H. YEE, *Extension of efficient low dissipation high-order schemes for 3D curvilinear moving grids*, Front. Comput. Fluid Dyn., (2002), pp. 129–164.
[29] T. NONOMURA, N. IIZUKA AND K. FUJII, *Freestream and vortex preservation properties of high-order WENO and WCNS on curvilinear grids*, Comput. Fluids, 39 (2010), pp. 197–214.
[30] R. VICHNEVETSKY AND J. B. BOWLES, Fourier Analysis of Numerical Approximations of Hyperbolic Equations, SIAM Philadelphia, 1982.
[31] X. LIU, X. DENG AND M. MAO, *High-order behaviors of weighted compact fifth-order nonlinear schemes*, AIAA J., 45(8) (2007).
[32] M. H. CARPENTER, D. GOTTLIEB AND S. ABARBANEL, *The stablity of numerical boundary treatments for compact high-order finite-difference schemes*, J. Comput. Phys., 108 (1993), pp. 272–295.
[33] D. KOSLOFF AND H. TAL-EZER, *A modified Chebyshev pseudo-spectral method with an $\mathcal{O}(1/n)$ time step restriction*, J. Comput. Phys., 104 (1993), pp. 457–469.
[34] H. LIU, X. DENG, M. MAO AND G. WANG, *High order nonlinear schemes for viscous terms and the application to complex configuration problems*, AIAA, (2011), 2011-369.
[35] J. CASPER, C. W. SHU AND H. ATKINS, *Comparision of two formulations for high-order accurate essentially nonoscillatory schemes*, AIAA J., 32(10) (1994).
[36] H. ATKINS AND J. CASPER, *Nonreflective boundary conditions for high-order methods*, AIAA J., 32(3) (1994).

https://doi.org/10.4208/aamm.2016.m1477 Published online by Cambridge University Press

[37] G. O. ROBERTS, *Computational meshes for the boundary problems*, in: Second International Conference Numerical Methods Fluid Dynamics, Lecture Notes in Physics (Springer-Verlag, New York, 1971).
[38] Z. J. WANG, K. FIDKOWSKI, R. ABGRALL, F. BASSI, D. CARAENI, A. CARY, H. DECONINCK, R. HARTMANN, K. HILLEWAERT, H. T. HUYNH, N. KROLL, G. MAY, P. O. PERSSON, B. VAN LEER AND M. VISBAL, *High-order CFD methods: current status and perspective*, Int. J. Numer. Meth. Fluids, 72 (2013), pp. 811–845.
[39] R. ABGRALL AND D. D. SANTIS, *Linear and non-linear high order accurate residual distribution schemes for the discretization of the steady compressible Navier-Stokes equations*, J. Comput. Phys., 283 (2015), pp. 329–359.
[40] N. KROLL, *Adigma–a European project on the development of adaptive higher-order variational methods for aerospace applications*, AIAA, (2009), 2009-176.
[41] T. LEICHT AND R. HARTMANN, *Error estimation and anisotropic mesh refinement for 3D laminar aerodynamic flow simulations*, J. Comput. Phys., 229 (2010), pp. 7344–7360.

https://doi.org/10.4208/aamm.2016.m1477 Published online by Cambridge University Press